Energy & Environmental Science

Accepted Manuscript

ROYAL SOCIETY OF CHEMISTRY

www.rsc.org/ees

Thermodynamic Limits of Extractable Energy by Pressure Retarded Osmosis

Energy and Environmental Science

Revised: May 19, 2014

Shihong Lin, Anthony P. Straub and Menachem Elimelech*

Department of Chemical and Environmental Engineering
Yale University
New Haven, Connecticut 06520-8286

*Corresponding author: email: menachem.elimelech@yale.edu; Tel. +1 (203) 432-2789;

Abstract

Salinity gradient energy, which is released upon mixing two solutions of different concentrations, is considered a promising source of sustainable power. Of the methods available to harvest salinity gradient energy, pressure retarded osmosis (PRO) has been one of the most widely investigated. In this study, we identify the thermodynamic limits of the PRO process by evaluating the obtainable specific energy, or extractable energy per total volume of the mixed solutions. Three distinct operation modes are analyzed: an ideal case for a reversible process, and constant-pressure operations with either co-current or counter-current flow in a membrane module. For module-scale operation, counter-current flow mode is shown to be more efficient than co-current flow mode. Additionally, two distinct thermodynamically limiting operation regimes are identified in counter-current flow mode — the draw limiting regime and the feed limiting regime. We derive analytical expressions to quantify the maximum specific energy extractable and the corresponding optimal feed flow rate fraction and applied pressure for each operation mode. Using the analytical expressions, we determine that maximum extractable energy in constant-pressure PRO with seawater (0.6 M NaCl) as a draw solution and river water (0.015 M NaCl) as a feed solution is 0.192 kWh per cubic meter of mixed solution (75% of the maximum specific Gibbs free energy of mixing). Considering this is the theoretical upper bound of extractable energy by the PRO process, we discuss further efficiency losses and energy requirements (e.g., pretreatment and pumping) that may render it difficult to extract a sizable net specific energy from a seawater and river water solution pairing. We analyze alternative source waters that provide higher salinity difference and hence greater extractable specific energy, such as reverse osmosis brine paired with treated wastewater effluent, which allow for a more immediately viable PRO process.

Broader Context

The concept of harnessing the energy released when two solutions of different salinities are mixed has been proposed as a promising source of clean energy. Pressure retarded osmosis (PRO) has been identified as one of the furthest developed methods to extract this energy of mixing and many studies have looked at the performance of small-scale membrane coupons in PRO. However, these coupon-sized experiments cannot give insight into the amount of energy extractable in the full-scale PRO process since, in practice, it is operated with membrane modules at a constant applied hydraulic pressure. We theoretically evaluate the PRO process to understand flow and concentration behavior in constant-pressure modules. Using this analysis, we establish the thermodynamic limit of extractable energy at the module scale. For river water mixing with the sea, one of the most widely considered source water pairings, we identify the maximum extractable energy in the process is 0.192 kWh per cubic meter of mixed total solution. Even though this is only 25% less than the Gibbs free energy of mixing, we discuss additional efficiency losses and energy costs that may substantially reduce the net specific energy available from the river water and seawater. We highlight other source water pairings for the PRO process which, in some cases, can circumvent the need for pretreatment and still offer relatively high efficiencies in a constant-pressure module.

Introduction

The quest for renewable energy has been accelerated in recent years by the urgent need to reduce greenhouse gas emissions and mitigate global warming.[1] In consequence, a variety of engineered systems have been conceived and developed to harness the energy constantly provided by nature. Salinity gradient energy, which is released upon mixing two solutions of different salt concentrations,[2] is considered a promising renewable energy source with an estimated global power potential of 1.4-2.6 TW.[3] In addition to its large potential, salinity gradient energy also has the theoretical advantage of relatively high volume power density. For instance, in a reversible thermodynamic process, the energy released from mixing a cubic meter of fresh water into the sea is estimated to be about 0.8 kWh,[4] which is equivalent to a hydraulic water head of ~290 meters.

Pressure retarded osmosis (PRO), reverse electrodialysis, and capacitive mixing are emerging processes to harvest salinity gradient energy.[3,5-10] Of these, PRO is the most widely investigated. In the PRO process, the chemical potential difference drives water from a low-salinity feed solution across a semipermeable membrane into a high-salinity draw solution. A hydraulic pressure lower than the osmotic pressure difference is applied to the draw solution and the incremental increase in volume (or flow rate) of the pressurized draw solution is used to drive a hydro-turbine and generate power.[11-14]

Most existing PRO studies were carried out at the scale of a membrane coupon with the goal of understanding the local mass transfer kinetics and membrane power density. [15-19] However, information from coupon level analysis cannot be used to predict the performance of the PRO process because, in practice, a PRO system comprises membrane modules and is operated at a constant applied hydraulic pressure[20]. In this operation mode, salt buildup in the feed solution and dilution of salts in the draw solution impose a thermodynamic limit on the extractable energy that is considerably lower than the efficiency of a reversible process. Similar thermodynamic limitations have been demonstrated for separation processes involving high salinity feed solutions, such as reverse osmosis[21,22] and direct contact

membrane distillation,[23] but PRO modeling at the module scale to establish the thermodynamic limits of the process has not been conducted yet. This type of analysis is critical to understand the efficiency of the process as well as to determine the optimal module configuration and operation conditions.

When quantifying energy efficiency of a PRO process, it is necessary to consider the method used to normalize the extractable energy. Previous analyses on salinity gradient energy mainly focused on the extractable energy per volume of feed (low salinity) solution, with the goal of evaluating the limit of available energy assuming fresh water as the scarce resource.[4,24,25] A straightforward conclusion with this approach is that the energy extractable per volume of feed solution will be maximized if the feed volume fraction (i.e. the initial volume of feed divided by the total volume of mixed solution) approaches zero. However, feed volume fraction approaching zero for maximizing the energy per volume of feed solution is an impractical operation condition in PRO, which provides no realistic rationale for process optimization with respect to feed volume fraction. In addition, while fresh water is indeed the limiting resource compared to the virtually inexhaustible seawater, Post et al. identified that there are economic costs associated with pretreating and transporting both the feed and draw solutions.[26] Therefore, from a practical point of view, a more reasonable metric is the extractable energy normalized by the total volume of the mixed solutions, which is hereby defined as *specific energy*.

In this paper, we evaluate the thermodynamic limits of the maximum specific energy extractable in a PRO process and determine the corresponding optimal operating conditions. Three different operation modes are analyzed: an ideal case for a reversible process, and constant-pressure operations with either co-current flow or counter-current flow in a membrane module. Our module-scale analysis identifies two distinct thermodynamically limiting operation regimes in counter-current flow operation: the draw limiting regime and the feed limiting regime. We also derive analytical expressions to quantify the optimal operating conditions and the corresponding maximum specific energy extractable in the

different operation modes. Practical implications for potential applications of PRO are discussed based on the theoretical limits of the maximum specific energy.

Thermodynamically Reversible PRO Process

The Gibbs free energy of mixing is the thermodynamic upper bound of the energy extractable by mixing two solutions of different salinities and can be attained only via a thermodynamically reversible process. In PRO, a thermodynamically reversible process can be realized in a batch mode by keeping the applied pressure infinitesimally smaller than the osmotic pressure difference throughout the entire process. It has been proven that the energy generated in such a reversible PRO process exactly equals the Gibbs free energy of mixing.[4] In this section, we discuss the Gibbs free energy of mixing per volume of mixed solution, ΔG_{V_M} (i.e. the specific Gibbs free energy of mixing), as a function of feed volume fraction, ϕ, with the goal of identifying the optimal ϕ that yields the maximum specific Gibbs free energy of mixing.

Specific Gibbs Free Energy of Mixing

The molar Gibbs free energy of mixing, $\Delta G_{mix,n_M}$, is defined as the energy per mole of mixed solution generated from mixing two solutions of different salinities in an isothermal and isobaric process.[27,28] It can be evaluated as the difference between the molar entropy after and before mixing:[26]

$$-\frac{\Delta G_{n_M}}{RT} = \sum_i x_{i,M} \ln(\gamma_{i,M} x_{i,M}) - \frac{n_F}{n_M} \sum_i x_{i,F} \ln(\gamma_{i,F} x_{i,F}) - \frac{n_D}{n_M} \sum_i x_{i,D} \ln(\gamma_{i,D} x_{i,D}) \quad (1)$$

Here, R is the ideal gas constant; T is the absolute temperature; n_M, n_F, and n_D are the total amount (in moles) of mobile species (i.e. solvent molecules, dissociated ions from solutes, and, if present, neutral solute molecules) in the mixed, feed, and draw solutions, respectively; $x_{i,M}$, $x_{i,F}$, and $x_{i,D}$ are the mole fractions of species "i" in the mixed, feed, and

draw solutions, respectively; and $\gamma_{i,M}$, $\gamma_{i,F}$, and $\gamma_{i,D}$ are the activity coefficients of species "i" in the corresponding solutions.

For dilute solutions, the activity coefficients can be approximated as unity.[29] Further, assuming negligible contribution of solute to the volume of the solution, the ratio of total moles in the feed and draw solutions to the total moles in the mixed solution (i.e. n_F/n_M and n_D/n_M, respectively) can be approximated by the corresponding volume fractions: $n_F/n_M \approx \phi$ and $n_D/n_M \approx 1-\phi$.[4] Applying these simplifications to eq 1 leads to an expression for the specific Gibbs free energy of mixing, ΔG_{V_M}, as a function of the molar concentrations of the feed, draw, and mixed solutions ($c_F, c_D,$ and c_M) as well as the feed volume fraction,[4] ϕ:

$$\frac{\Delta G_{V_M}}{\nu RT} = c_M \ln(c_M) - \phi c_F \ln(c_F) - (1-\phi) c_D \ln(c_D) \qquad (2)$$

where ν is the van't Hoff factor for strong electrolytes (e.g., $\nu = 2$ for NaCl).

Fig. 1 presents the specific Gibbs free energy of mixing as a function of the feed volume fraction, ϕ, as predicted by the more precise eq 1 (open symbols) and the simplified eq 2 (dashed lines). The simplified equation (eq 2) always overestimates ΔG_{V_M} as compared to eq 1. The absolute deviation is more significant when ΔG_{V_M} is higher, but is always less than 10% of ΔG_{V_M}. The optimal feed volume fractions are very similar from the predictions by both the precise and simplified equations. Therefore, hereafter we will only use the simplified equation (eq 2) for the convenience of derivation.

FIGURE 1

Optimal Feed Fraction and Maximum Specific Energy

In a thermodynamically reversible PRO process, the feed volume fraction, ϕ, is the only operational parameter. The maximum ΔG_{V_M} occurs when its derivative with respect to ϕ is zero:

$$\frac{d\left(\Delta G_{V_M}\right)}{d\phi} = 0 \quad (3)$$

Solving eq 3 using the simplified expression for ΔG_{V_M} (eq 2) leads to the critical feed fraction, $\phi_{cr,\Delta G}$, with which the specific Gibbs free energy of mixing is maximized:

$$\phi_{cr,\Delta G} = \frac{exp\left(\frac{c_F \ln(c_F) - c_D \ln(c_D)}{c_F - c_D} - 1\right) - c_D}{c_F - c_D} \quad (4)$$

Combining eq 2 and eq 4 yields the maximum specific Gibbs free energy, $\Delta G_{V_M,max}$:

$$\frac{\Delta G_{V_M.max}}{\nu RT} = \frac{c_D c_F}{c_D - c_F}(\ln(c_D) - \ln(c_F)) - exp\left(\frac{c_D \ln(c_D) - c_F \ln(c_F)}{c_D - c_F} - 1\right) \quad (5)$$

Both $\phi_{cr,\Delta G}$ and $\Delta G_{V_M.max}$ are simply functions of the feed and draw concentrations, c_F and c_D, respectively. Thorough inspection of calculated $\phi_{cr,\Delta G}$ over a wide range of reasonable feed and draw concentrations reveals that $\phi_{cr,\Delta G}$ is mostly centered around 0.6 and decreases slightly for higher feed concentrations (Fig. S1).

Module-Scale PRO Analysis

While the Gibbs free energy of mixing represents the theoretical upper bound of extractable energy, it is difficult to approach in practice, as it requires a thermodynamically reversible process where the applied pressure always equals the varying osmotic pressure difference between the feed and draw solutions. A full-scale PRO process operates with membrane modules under constant pressure. In this section, we describe the mass transfer in a PRO module that is of either counter-current or co-current flow configuration. The goal is to understand the impacts of two major operation parameters — the applied hydraulic pressure, ΔP, and the feed flow rate fraction, ϕ — on the performance of PRO at the module scale.

Because we are interested in understanding the thermodynamic limits of system performance, we deliberately ignore non-idealities in conducting our system scale analysis. Specifically, the idealizing assumptions include (i) absence of reverse draw salt flux, which implies a membrane with perfect selectivity, and (ii) absence of internal and external

concentration polarizations, which is equivalent to having a membrane with a negligible structural parameter and operating the PRO process with perfect hydrodynamics (i.e., complete mixing). As will be shown in the subsequent sections, ignoring non-idealities enables the derivation of simple analytical expressions for the upper bound of extractable energy and the corresponding operating conditions. With these underlying assumptions, the ideal trans-membrane water flux, $J_{W,i}$, can be related to the bulk concentration difference by the following equation:

$$J_{W,i}(c_D, c_F) = A[\pi(c_D) - \pi(c_F) - \Delta P] \quad (6)$$

where A is the pure water permeability of the PRO membrane and $\pi(c)$ is the osmotic pressure of a solution of molar concentration c. To further simplify our analysis, we assume the osmotic pressure as a function of molar concentration following the van't Hoff equation:

$$\pi(c) = \nu RTc \quad (7)$$

We note that predictions based on this equation deviate slightly from the actual osmotic pressure when the solution is highly concentrated.[30]

Mass Transfer in Counter-current Flow

The mass balance of water and of draw solute in a counter-current flow module is given by:

$$\frac{dQ_D}{ds} = J_{W,i}(c_D(s), c_F(s)) \quad (8A)$$

$$\frac{dQ_F}{ds} = J_{W,i}(c_D(s), c_F(s)) \quad (8A)$$

$$c_D(s) = \frac{c_{D,0}Q_{D,0}}{Q_D(s)} \quad (8C)$$

$$c_F(s) = \frac{c_{F,0}Q_{F,0}}{Q_F(s)} \quad (8D)$$

Specifically, eqs 8A and 8B quantify the mass transfer of water across the semi-permeable membrane, and eqs 8C and 8D describe the mass balance of draw solute in the draw and feed solutions, with the assumption that the membrane perfectly rejects the draw solute. The

position in the module is represented by the normalized membrane area, s, which is defined as the membrane area between the entrance of the draw solution stream (as the convention in this paper) and the position being described, normalized by the total membrane area in the module. Using s to quantify the relative position in the module eliminates the need to specify the configuration of the cross section and the membrane area per unit length of module, and thus renders the analysis generally applicable.

For module-scale operation in counter-current configuration with a total membrane area, σ, the boundary conditions are $c_D(0) = c_{D,0}$ and $Q_D(0) = Q_{D,0}$ (i.e. $s = 0$ corresponds to the draw solution entrance), and $c_F(\sigma) = c_{F,0}$ and $Q_F(\sigma) = Q_{F,0}$ (i.e. $s = \sigma$ corresponds to the feed solution entrance).

Mass Transfer in Co-current Flow

The mass balance of water and of draw solute in a co-current flow module is given by

$$\frac{dQ_D(s)}{ds} = J_{W,i}(c_D(s), c_F(s)) \quad (9A)$$

$$\frac{dQ_F(s)}{ds} = -J_{W,i}(c_D(s), c_F(s)) \quad (9B)$$

$$c_D(s) = \frac{c_{D,0}Q_{D,0}}{Q_D(s)} \quad (9C)$$

$$c_F(s) = \frac{c_{F,0}Q_{F,0}}{Q_F(s)} \quad (9D)$$

Note that these equations that describe the mass balance in a co-current flow module are almost the same as those for the counter-current flow module (eq 8), except for eq 9B due to the different flow direction. The boundary conditions for the co-current flow operation are $c_D(0) = c_{D,0}$ and $Q_D(0) = Q_{D,0}$, and $c_F(0) = c_{F,0}$ and $Q_F(0) = Q_{F,0}$ (i.e. $s = 0$ corresponds to the entrances for both the feed and draw solutions).

Operation Regimes in the PRO Module

Solving the mass balance equations (eqs 8 and 9) yields the flow rate and solute concentration distributions along the modules. The solute concentration distributions for both counter-current (dashed curves) and co-current (solid curves) configurations are presented in Fig. 2C and 2D for different initial feed flow rate fractions, ϕ. To be more general, instead of showing the flow rate distributions, Fig. 2A and 2B show the distribution of flow rate fractions which are independent of the absolute flow rates of the system. In Fig. 2, the membrane area, σ, pure water permeability, A, and feed flow rate, $Q_{F,0}$, are deliberately chosen so that mass transfer can proceed to the thermodynamic limit. The extent of mass transfer is characterized the by the parameter $\chi = A\sigma/Q_{F,0}$. Note that for a given feed concentration, draw concentration, and applied hydraulic pressure, the flow rate fraction and solute concentration distribution profiles will remain identical as long as the χ value is unchanged. Completion of mass transfer in Fig. 2 is indicated by the existence of a portion of the membrane module where both the flow rate fractions and solute concentrations remain constant. In such portions of the membrane module, the driving force for mass transfer (i.e., the difference between the osmotic pressure difference and the applied hydraulic pressure) vanishes so that the trans-membrane water flux given by eq 6 becomes zero.

FIGURE 2

For co-current flow operation, both the draw solute concentration decreases and the feed concentration increases considerably along the module with a small feed flow rate fraction $\phi = 0.3$ (Fig. 2C). However, with $\phi = 0.8$, a relatively large value, the feed concentration barely changes (Fig. 2D) because only a small fraction of the water from the feed solution transfers across the membrane before the draw concentration decreases to the level that the condition for zero driving force is reached. For counter-current flow operation, there are two distinct operation regimes, depending on the initial feed flow rate fraction, ϕ. When ϕ is small (e.g. $\phi = 0.3$), the feed concentration increases to a critical feed concentration, c_F^* (Fig. 2C), which is dependent on the initial draw concentration, $c_{D,0}$, and the applied hydraulic pressure, ΔP:

$$c_F^* \equiv c_{D,0} - \frac{\Delta P}{\nu RT} \quad (10)$$

The driving force vanishes when c_F reaches c_F^*, as the osmotic pressure difference is equal to the applied hydraulic pressure. A counter-current flow PRO operation with its effluent feed concentration, $c_{F,f}$, reaching the critical feed concentration, c_F^*, is considered to be in the *feed limiting regime* (FLR). In contrast, when ϕ is large (e.g. $\phi = 0.8$), the draw concentration, c_D, decreases to a critical draw concentration, c_D^* (Fig. 2D), which is a function of the initial feed concentration, $c_{F,0}$, and the applied pressure, ΔP:

$$c_D^* \equiv c_{F,0} + \frac{\Delta P}{\nu RT} \quad (11)$$

Eq 11 corresponds to a thermodynamic equilibrium in which the osmotic pressure difference between the solutions of c_D^* and $c_{F,0}$ is equal to the applied hydraulic pressure. Analogously, we identify a PRO operation in which the effluent draw concentration, $c_{D,f}$, reaches the critical draw concentration, c_D^*, as an operation in the *draw limiting regime* (DLR). We note that similar concepts of thermodynamically limiting regimes have been identified in module scale operation of reverse osmosis[21] and direct contact membrane distillation, [23] in which the driving force for mass transfer decreases as the process proceeds.

Regardless of the flow configuration and operation regime, the specific energy of the operation, w, is always defined as the power extractable from the system, $\dot{W}$, normalized by the total flow rate, Q_{Tot}:

$$w = \frac{\dot{W}}{Q_{Tot}} = \frac{\Delta P \Delta Q}{Q_{D,0} + Q_{F,0}} = \Delta P \phi \gamma(\Delta P, \phi) \quad (12)$$

where ΔQ is the trans-membrane flow rate (i.e. the integral of water flux with respect to the membrane area for the entire module) and γ is the feed recovery rate, defined as the ratio of ΔQ over the initial feed flow rate $Q_{F,0}$. For a given PRO system, the feed recovery rate, γ, is a function of both the applied pressure, ΔP, and the initial feed flow rate fraction, ϕ. It is worth noting that in both cases presented in Fig. 2 ($\phi = 0.3$ and $\phi = 0.8$), the feed recovery

rates are very similar for co-current and counter-current operations, which, as we will show later, is not necessarily the case with an intermediate ϕ.

The specific energy normalization shown above assigns equal value to feed and draw solutions, an assumption that has been made previously[25] and allows for the derivation of simple analytical equations. However, in reality, the normalization should take into account the difference between the feed and draw solutions in their relative energetic cost of procurement, pretreatment, and pumping. This type of extensive analysis, while useful, is beyond the scope of this work.

Thermodynamic Analysis of Limiting Regimes

From the numerical solution of eq 8, as presented in Fig. 2, we have identified two distinct regimes (FLR and DLR) for PRO operation with counter-current flow configuration. It appears that as long as the membrane area is sufficiently large so that these thermodynamic limiting regimes are reached, the performance of the system can be analytically determined based on simple mass balance with eqs 10-12.

When the PRO operation is in FLR, mass balance and the condition $c_{F,f} = c_F^*$ dictate the feed recovery rate, γ_{FLR}:

$$\gamma_{FLR} = 1 - \frac{c_{F,0}}{c_F^*} \tag{13}$$

The specific energy in FLR is then given by

$$w_{FLR} = \Delta P \phi \gamma_{FLR} = \Delta P \phi \left(1 - \frac{c_{F,0}}{c_F^*}\right) \tag{14}$$

In FLR, both the boundary conditions $c_{F,f} = c_F^*$ and $c_{D,f} \geq c_D^*$ should be satisfied, which leads to the necessary operation condition:

$$\phi \leq \phi_{FLR} = \frac{c_F^*}{c_{D,0} + c_{F,0}} \tag{15}$$

We note that c_F^* and c_D^* are both functions of ΔP, and therefore, ϕ_{FLR} is a function of $c_{F,0}$, $c_{D,0}$, and ΔP.

Analogously, when the PRO operation is in DLR, the feed recovery rate, γ_{DLR}, can be readily determined by mass balance and the condition $c_{D,f} = c_D^*$:

$$\gamma_{DLR} = \frac{1-\phi}{\phi}\left(\frac{c_{D,0}}{c_D^*} - 1\right) \quad (16)$$

The specific energy in DLR is then given by

$$w_{DLR} = \Delta P \phi \gamma_{DLR} = \Delta P (1-\phi)\left(\frac{c_{D,0}}{c_D^*} - 1\right) \quad (17)$$

The necessary conditions for a PRO to operate in DLR can be determined by the boundary conditions that $c_{D,f} = c_D^*$ and $c_{F,f} \leq c_F^*$:

$$\phi \geq \phi_{DLR} = \frac{c_F^*}{c_{D,0} + c_{F,0}} \quad (18)$$

Comparing eqs 15 and 18 reveals that under the same applied pressure as well as feed and draw concentrations, ϕ_{DLR} is exactly equal to ϕ_{FLR}, which means that such a critical initial feed flow rate fraction, ϕ^* ($\phi^* = \phi_{FLR} = \phi_{DLR}$), demarcates operation in both FLR and DLR as long as there is sufficient membrane area for the operation to reach the thermodynamic limiting regimes. If the membrane area is insufficient, the condition of zero driving force will not be reached anywhere in the module. Consequentially, the effluent feed concentration will always be lower than c_F^*, and the effluent draw concentration will always be higher than c_D^*.

Finally, it should be noted that the above analysis on thermodynamic limiting regimes is only applicable for counter-current flow operation, in which the equilibrium condition can occur on either end of the module. In the special case of $\phi = \phi^*$, the equilibrium occurs on both ends of the module simultaneously. In a co-current flow operation, although the concentration distributions seem to be very different between the case when ϕ is small and that when ϕ is large, there is no distinctive operation regime that can be defined in a way similar to that of the counter-current flow operation, because the equilibrium condition can only occur at the exit of the module.

Optimal Conditions for Module Operation

The analysis of thermodynamic limiting operation regimes presented above is important for understanding the behavior of a counter-current flow PRO process at a module scale. In addition, eqs 14 and 17 allow us to evaluate the specific energy of the process, which, for given sources of feed and draw solutions, is dependent on the applied pressure, ΔP, and the initial feed flow rate fraction, ϕ. In this section, we will identify the optimal operation conditions and the corresponding maximum specific energy for both counter-current and co-current flow operation.

Counter-Current Flow Operation

Because the specific energy in FLR, $w_{FLR}(\phi)$ (eq 14), is a monotonically increasing function, and the upper bound of ϕ in FLR is ϕ_{FLR} (eq 15), the optimal ϕ in FLR is ϕ_{FLR}, and the maximum specific energy is $w_{FLR}(\phi_{FLR})$. Analogously, since the specific energy in DLR, $w_{DLR}(\phi)$ (eq 17), is a monotonically decreasing function, and the lower bound of ϕ in DLR is ϕ_{DLR} (eq 18), the optimal ϕ in DLR is ϕ_{DLR}, and the maximum specific energy is $w_{DLR}(\phi_{DLR})$. However, it has been shown that ϕ_{FLR} is exactly equal to ϕ_{DLR} for a given applied pressure and a given set of working concentrations ($c_{D,0}$ and $c_{F,0}$). Therefore, the optimal initial feed flow rate fraction in a counter-current flow operation ($\phi_{opt,CT}$) is the critical feed flow rate (ϕ^*) that divides the FLR and DLR:

$$\phi_{opt,CT}(\Delta P) = \frac{c_D^*}{c_{D,0} + c_{F,0}} = \frac{c_{D,0} - \Delta P/(\nu RT)}{c_{D,0} + c_{F,0}} \tag{19}$$

The corresponding maximum specific energy is then given by either $w_{DLR}(\phi^*)$ or $w_{FLR}(\phi^*)$, with both yielding the same analytical equation:

$$w_{max,CT}(\Delta P) = \Delta P \frac{c_{D,0} - c_{F,0} - \Delta P/(\nu RT)}{c_{D,0} + c_{F,0}} \tag{20}$$

The optimal initial feed flow rate fraction and the corresponding maximum specific energy are plotted in Fig. 3 as functions of the applied pressure, ΔP.

FIGURE 3

The blue dashed curve in Fig. 3 gives the maximum specific energy extractable for a given applied hydraulic pressure, which can be considered as the local maximum attainable if the initial feed flow rate fraction is optimally tailored to a given pressure. However, there also exists an optimal applied pressure that leads to a global maximum of the specific energy. From observing the maximum specific energy curve (Fig. 3) and also inspecting the structure of eq 20, it is evident that the global maximum of specific energy occurs when the applied pressure is half of the osmotic pressure difference (i.e. $\Delta P = \nu RT\left(c_{D,0} - c_{F,0}\right)/2$). This is also well known as the condition for achieving a maximum power density for a small membrane coupon (i.e. not at the module scale)[15]. However, it should be emphasized that the underlying principles behind these two optimal conditions are totally different.

When the applied pressure is half of the osmotic pressure difference, the corresponding optimal initial feed flow rate fraction is $\phi_{\mathrm{opt,CT}}(\Delta\pi/2) = 0.5$. In other words, the conditions leading to a global maximum of specific energy are $\Delta P = \Delta\pi/2$ and $\phi = 0.5$. Applying these conditions to either eq 14 or 17 yields the expression for the maximum specific energy of PRO in counter-current flow configuration, $w^*_{max,CT}$:

$$w^*_{max,CT} = w_{max,CT}\left(\frac{\Delta\pi}{2}\right) = \frac{\nu RT}{4}\frac{(c_{D,0} - c_{F,0})^2}{(c_{D,0} + c_{F,0})} \tag{21}$$

As a global maximum, $w^*_{max,CT}$ is simply a function of the initial feed and draw concentrations as well as the working temperature.

Co-Current Flow Operation

For co-current flow operation, no distinct operation regimes can be defined as in counter-current flow operation. The specific energy for a module scale constant pressure PRO operation, regardless of operation mode, is always given by eq 12. In a co-current flow operation, the feed recovery, γ_{CO}, can be determined from

$$\Delta P = \nu RT\left(\frac{1/\phi - 1}{1/\phi - 1 + \gamma_{CO}}c_{D,0} - \frac{1}{1 - \gamma_{CO}}c_{F,0}\right) \tag{22}$$

The analytical expression of γ_{CO} as a function ΔP and ϕ based on eq 22 is too complicated to derive a simple analytical expression for an optimal initial feed flow rate fraction, $\phi_{opt,CO}$, as a function of the applied pressure, ΔP. However, the specific energy as defined by eq 12 can be readily solved numerically with different ΔP and ϕ. From the numerical results shown in Fig. 4, the global optimal operation conditions for co-current flow PRO operation are identified as $\Delta P = \Delta\pi/2$ and $\phi = 0.5$, which are exactly the same as those for counter-current flow operation. The global maximum of specific energy, $w^*_{max,CO}$, under these optimal operation conditions is given by

$$w^*_{max,CO} = w_{CO}(\Delta P = \frac{\Delta\pi}{2}, \phi = \frac{1}{2}) = \frac{\nu RT}{4}\left(\sqrt{c_{D,0}} - \sqrt{c_{F,0}}\right)^2 \quad (23)$$

FIGURE 4

It can be readily proven, by comparing eq 21 and 23, that under optimal conditions, operation in counter-current flow mode always yields a higher specific energy than that in co-current flow mode:

$$w^*_{max,CT} \geq w^*_{max,CO} \quad (24)$$

The only condition for the equality to hold is that $c_{D,0} = c_{F,0}$, which is a trivial condition as no mixing energy is extractable from the system with two streams of equal salinity.

Implications

Based on our preceding analysis, the analytical expressions for the optimal operating conditions and the corresponding maximum specific energy in the three different operation modes are summarized in Table 1. The optimal operating conditions and the maximum specific energy are both functions of the initial feed and draw concentrations as well as the working temperatures, and are independent of any properties of the module, except for the assumption of having sufficiently large membrane area. The expressions summarized in Table 1 can be used for facile evaluation of the maximum specific energy in different operation modes for given sources of water.

TABLE 1

Comparisons between the maximum specific energy at different operation modes using the expressions in Table 1 are presented in Fig. 5A for different combinations of feed and draw solutions. Depending on the specific combinations, a counter-current flow PRO process can yield a maximum specific energy that is about 70-90% of the specific Gibbs free energy of mixing, $\Delta G_{V_M,max}$, and a co-current flow PRO process can, at best, harvest 50-60% of $\Delta G_{V_M,max}$.

FIGURE 5

For constant pressure PRO with seawater (SW) as draw solution and river water (RW) as feed solution (Fig. S2), the theoretical maximum specific energy is 0.192 kWh/m^3 (i.e. 75% of the maximum specific Gibbs free energy of mixing, 0.256 kWh/m^3) with the chosen concentrations (0.015 M for RW and 0.6 M for SW). This theoretical maximum is predicted by assuming the absence of detrimental effects, such as reverse draw flux as well as internal and external concentration polarizations, which would further reduce the maximum specific energy. In addition, a PRO system will require pretreatment to mitigate fouling that would, in the long run, undermine membrane performance. While the extent of pretreatment is dependent on a variety of factors, the energetic cost may be as high as conventional water treatment[31] or seawater RO pretreatment,[32] making it comparable to, if not more than, the maximum specific energy of the PRO process. From this perspective, the energy loss from constant-pressure PRO operation may have a significant impact on the net specific energy obtainable in the process. This energetic loss in conjunction with the pretreatment requirements, pumping energy costs to circulate the feed and draw solutions, inefficiencies in the hydroturbine and pressure exchanger, and the aforementioned losses due to non-ideal membranes may render it very challenging to harvest a sizable amount of energy in river water and seawater PRO. However, with significant advances in the understanding of pretreatment requirements and innovative systems designed to minimize efficiency losses, a viable net energy output may still be achieved.

While harvesting the energy of mixing between SW and RW using PRO may be difficult with current technologies, alternative salinity gradients may offer greater immediate potential in PRO (Fig. 5A). For example, Great Salt Lake water (~27% salinity in its highest concentration region, approximately equal to 4.6 M NaCl) has been proposed as draw solution to work with river water (~0.015 M NaCl) as feed solution,[33] which can yield theoretical maximum specific energy of ~1.6 kWh/m^3 with counter-current flow PRO (eq 21, with $\phi = 0.5$). Another potential combination entails using Dead Sea water (~33.7% salinity, approximately equivalent to ~5.7 M NaCl) as draw solution and RO brine as feed solution (~1.2 M NaCl),[34] which can yield a maximum ideal specific energy of about 1.0 kWh/m^3 using counter-current flow PRO (eq 21, with $\phi = 0.5$). Note that pretreatment is not necessary in the second case for the RO brine feed solution, as it has been pretreated prior to the RO process. In both cases, sizable net energy output per volume of mixed solution can be attained even after considering the non-idealities that significantly reduce the specific energy. Fig. 5B shows the maximum specific energy in counter-current flow mode as a function of draw and feed solution concentrations and can be used to evaluate additional solution pairings. Tapping into energy sources of high salinity requires PRO operation under high pressure that has been experimentally demonstrated to be feasible.[35]

Beyond harnessing energy from natural salinity gradients, PRO shows promise as an energy recovery component in hybrid engineered systems. For example, the Mega-ton project in Japan uses PRO to recover energy from mixing RO brine (draw solution) and treated wastewater effluent (feed solution) to supplement the energy input for the RO process (maximum specific energy of ~0.4 kWh/m^3 with counter-current flow as shown in Fig. 5).[36] Extensive pretreatment is unnecessary in this case, because the draw and feed solutions have been treated in the preceding processes. Furthermore, the system has the added benefit of abating the environmental impact of the discharged RO brine.

References

1. M. I. Hoffert, *Science*, 2002, **298**, 981–987.
2. B. E. Logan and M. Elimelech, *Nature*, 2012, **488**, 313–319.
3. G. Z. Ramon, B. J. Feinberg, and E. M. V. Hoek, *Energy Environ. Sci.*, 2011, **4**, 4423–4434.
4. N. Y. Yip and M. Elimelech, *Environ. Sci. Technol.*, 2012, **46**, 5230–5239.
5. J. W. Post, J. Veerman, H. V. M. Hamelers, G. J. W. Euverink, S. J. Metz, K. Nymeijer, and C. J. N. Buisman, *J. Membr. Sci.*, 2007, **288**, 218–230.
6. D. A. Vermaas, E. Guler, M. Saakes, and K. Nijmeijer, *Energy Procedia*, 2012, **20**, 170–184.
7. D. A. Vermaas, J. Veerman, N. Y. Yip, M. Elimelech, M. Saakes, and K. Nijmeijer, *ACS Sustainable Chem. Eng.*, 2013, **1**, 1295–1302.
8. M. Bijmans, O. S. Burheim, M. Bryjak, and A. Delgado, *Energy Procedia*, 2012.
9. R. A. Rica, R. Ziano, D. Salerno, and F. Mantegazza, *Entropy*, 2013.
10. M. C. Hatzell, R. D. Cusick, and B. Logan, *Energy Environ. Sci.*, 2014.
11. S. E. Skilhagen, J. E. Dugstad, and R. J. Aaberg, *Desalination*, 2008, **220**, 476–482.
12. A. Achilli, T. Y. Cath, and A. E. Childress, *J. Membr. Sci.*, 2009, **343**, 42–52.
13. A. Achilli and A. E. Childress, *Desalination*, 2010, **261**, 205–211.
14. F. Helfer, C. Lemckert, and Y. G. Anissimov, *J. Membr. Sci.*, 2014, **453**, 337–358.
15. K. L. Lee, R. W. Baker, and H. K. Lonsdale, *J. Membr. Sci.*, 1981, **8**, 141–171.
16. T. Thorsen and T. Holt, *J. Membr. Sci.*, 2009, **335**, 103–110.
17. N. Y. Yip, A. Tiraferri, W. A. Phillip, J. D. Schiffman, and M. Elimelech, *Environ. Sci. Technol.*, 2010, **44**, 3812–3818.
18. N. Y. Yip and M. Elimelech, *Environ. Sci. Technol.*, 2011, **45**, 10273–10282.
19. Q. She, X. Jin, and C. Y. Tang, *J. Membr. Sci.*, 2012, **401-402**, 262–273.
20. Y. C. Kim, Y. Kim, D. Oh, and K. H. Lee, *Environ. Sci. Technol.*, 2013, **47**, 2966–2973.
21. L. Song, J. Y. Hu, S. L. Ong, W. J. Ng, M. Elimelech, and M. Wilf, *Desalination*, 2003, **155**, 213–228.
22. L. Song, J. Y. Hu, S. L. Ong, W. J. Ng, M. Elimelech, and M. Wilf, *J. Membr. Sci.*, 2003, **214**, 239–244.
23. S. Lin, N. Y. Yip, and M. Elimelech, *J. Membr. Sci.*, 2014, **453**, 498–515.
24. R. S. Norman, *Science*, 1974, **186**, 350–352.
25. J. N. Weinstein and F. B. Leitz, *Science*, 1976, **191**, 557–559.
26. J. W. Post, H. V. M. Hamelers, and C. J. N. Buisman, *Environ. Sci. Technol.*, 2008, **42**, 5785–5790.
27. S. I. Sandler, *Chemical and Engineering Thermodynamics*, Wiley, 1998.
28. J. M. Smith, H. Van Ness, and M. M. Abbott, *Introduction to Chemical Engineering Thermodynamics*, McGraw-Hill Professional, 2005.
29. R. A. Robinson and R. H. Stokes, *Electrolyte Solutions*, Courier Dover Publications, 2002.
30. A. D. Wilson and F. F. Stewart, *J. Membr. Sci.*, 2013, **431**, 205–211.
31. G. Klein, M. Krebs, V. Hall, T. O'Brien, and B. B. Blevins, *California Energy Commission (Ed)*, 2005.
32. C. Fritzmann, J. Löwenberg, T. Wintgens, and T. Melin, *Desalination*, 2007, **216**, 1–76.
33. S. Loeb, *Desalination*, 2001, **141**, 85–91.

34. S. Loeb, *Desalination*, 1998, **120**, 247–262.
35. A. P. Straub, N. Y. Yip, and M. Elimelech, *Environ. Sci. Technol. Lett.*, 2014, **1**, 55–59.
36. M. Kurihara and M. Hanakawa, *Desalination*, 2013, **308**, 131–137.

FIGURE CAPTIONS

Fig. 1. Specific Gibbs free energy of mixing (i.e. the reversible energy of mixing per volume of mixed feed and draw solutions) for waters of different sources as a function of the feed volume fraction, ϕ, defined as the ratio of feed solution to the mixed solution that includes both the feed and draw solutions. The following sources of waters were considered: seawater (SW, 0.6 M NaCl), river water (RW, 0.015 mM NaCl), brackish water (BW, 0.05 M NaCl), wastewater effluent (WW, 0.015 mM NaCl), and brine (1.2 M NaCl). The dash and dotted curves were obtained using the simplified molarity based equation (eq 2), whereas the open symbols are calculated using the more precise equation (eq 1).

Fig. 2. Distribution of flow rate fractions along a membrane module for feed (black) and draw (red) in counter-current flow mode (solid curves) and co-current flow mode (dashed curves) with (A) $\phi = 0.3$ and (B) $\phi = 0.8$, and corresponding distributions of solute concentrations of feed (black) and draw (red) in co-current flow mode (dashed curves) and counter-current flow mode (solid curves) with (C) $\phi = 0.3$ and (D) $\phi = 0.8$. The feed solution is river water (0.015 M) and the draw solution is seawater (0.6 M). The feed flow rate ,$Q_{F,0}$, membrane total area, σ, and pure water permeability, A, satisfy the condition that $\chi = A\sigma/Q_{F,0} = 0.2$ bar^{-1}. Note that χ characterizes the extent of mass transfer.

Fig. 3. Optimal feed flow rate fraction, ϕ, (red solid line, left axis) and the corresponding maximum specific energy (blue dashed curve, right axis) at different applied hydraulic pressures, ΔP, for PRO in counter-current flow mode under constant pressure. The black dotted line indicates the global optimal specific energy and operating conditions ($\phi = 0.5$, $\Delta P = \pi/2$). The feed solution is river water (0.015 M) and the draw solution is seawater (0.6 M). It is assumed that membrane area is sufficiently large so that the mixing proceeds to completion.

Fig. 4. Specific energy as a function of applied pressure, ΔP, and feed flow rate fraction, ϕ, for PRO in co-current flow mode under constant pressure. The feed solution is river water (0.015 M) and the draw solution is seawater (0.6 M). It is assumed that membrane area is sufficient so that the mixing proceeds to completion. The optimal applied pressure for a given feed flow rate fraction, ϕ, is shown with a dotted line. The white star indicates the global optimal condition that leads to the highest specific energy.

Fig. 5. (A) Maximum specific energy obtainable in PRO for three different cases: thermodynamically reversible PRO process (red), constant-pressure PRO in counter-current flow mode (blue), and constant-pressure PRO in co-current flow mode (green). The percentages of the maximum specific energy obtained in counter-current (blue) and co-current (red) modes (with reference to the ideal thermodynamically reversible PRO process, red bars in kWh/m^3) are indicated for each pairing of source waters. (B) Maximum specific energy in counter-current flow mode as a function of draw and feed solution concentrations. The salinities of seawater (SW), river water or wastewater (RW or WW), seawater reverse osmosis brine, Dead Sea water, and Great Salt Lake water are specified to be 0.6, 0.015, 1.2, 5.7, and 4.6 M NaCl, respectively. The temperature used in modeling was 25°C.

Table 1. Summary of analytical expressions for optimal operation conditions and the corresponding maximum specific energies in different operation modes.

	Optimal Operation Conditions		Maximum Specific Energy (νRT)
Reversible Process	$\phi = \frac{exp\left(\frac{c_F \ln(c_F) - c_D \ln(c_D)}{c_F - c_D} - 1\right) - c_D}{c_F - c_D}$		$exp\left(\frac{c_D \ln(c_D) - c_F \ln(c_F)}{c_D - c_F} - 1\right) - \frac{c_D c_F}{c_D - c_F}(\ln(c_D) - \ln(c_F))$
Constant Pressure	Counter -Current	$\phi = 1/2$ $\Delta P = \Delta\pi/2$	$\frac{1}{4}\frac{(c_D - c_F)^2}{(c_D + c_F)}$
	Co-Current	$\phi = 1/2$ $\Delta P = \Delta\pi/2$	$\frac{(\sqrt{c_D} - \sqrt{c_F})^2}{4}$

Note: For simplicity, the initial draw and feed concentrations in this table are expressed as c_D and c_F, respectively (instead of $c_{D,0}$ and $c_{F,0}$ as in the main text).

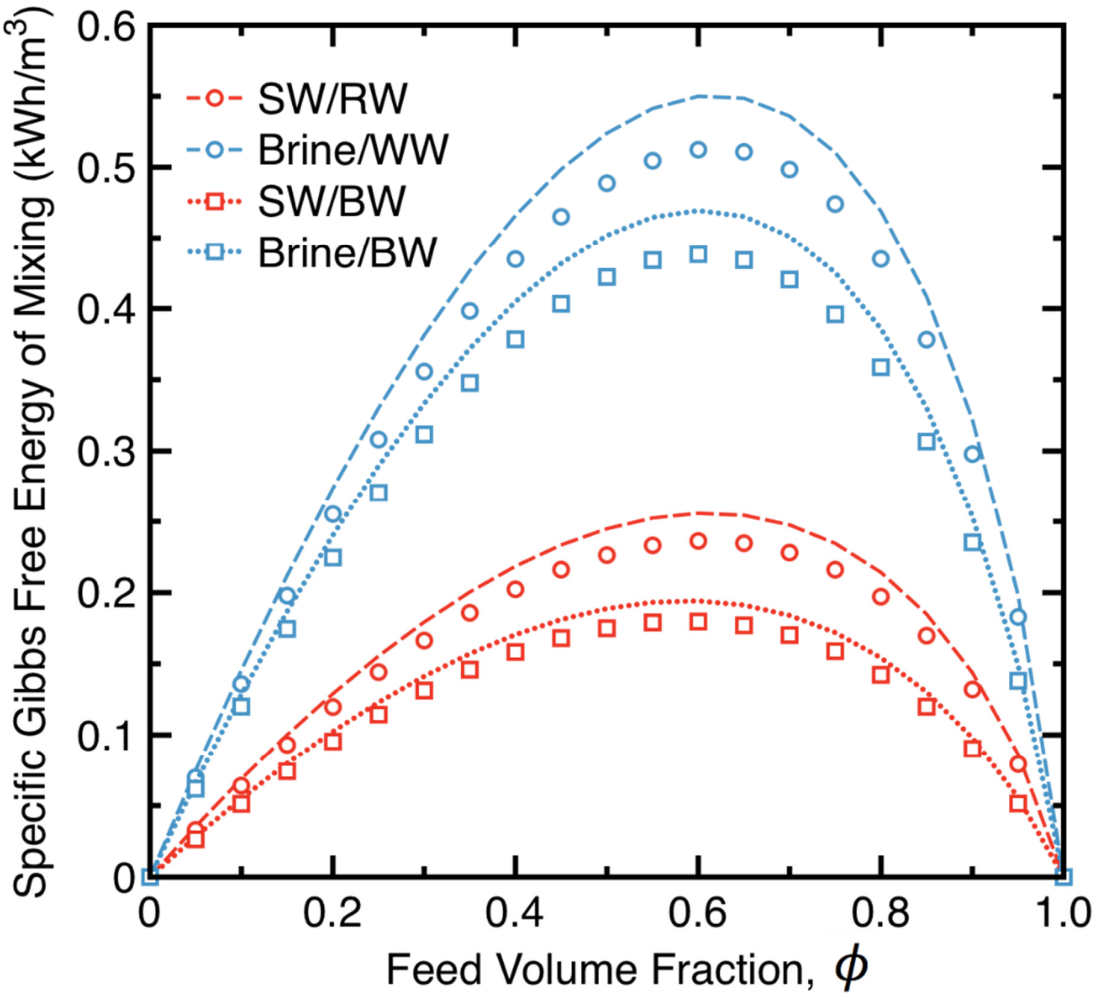

Figure 1

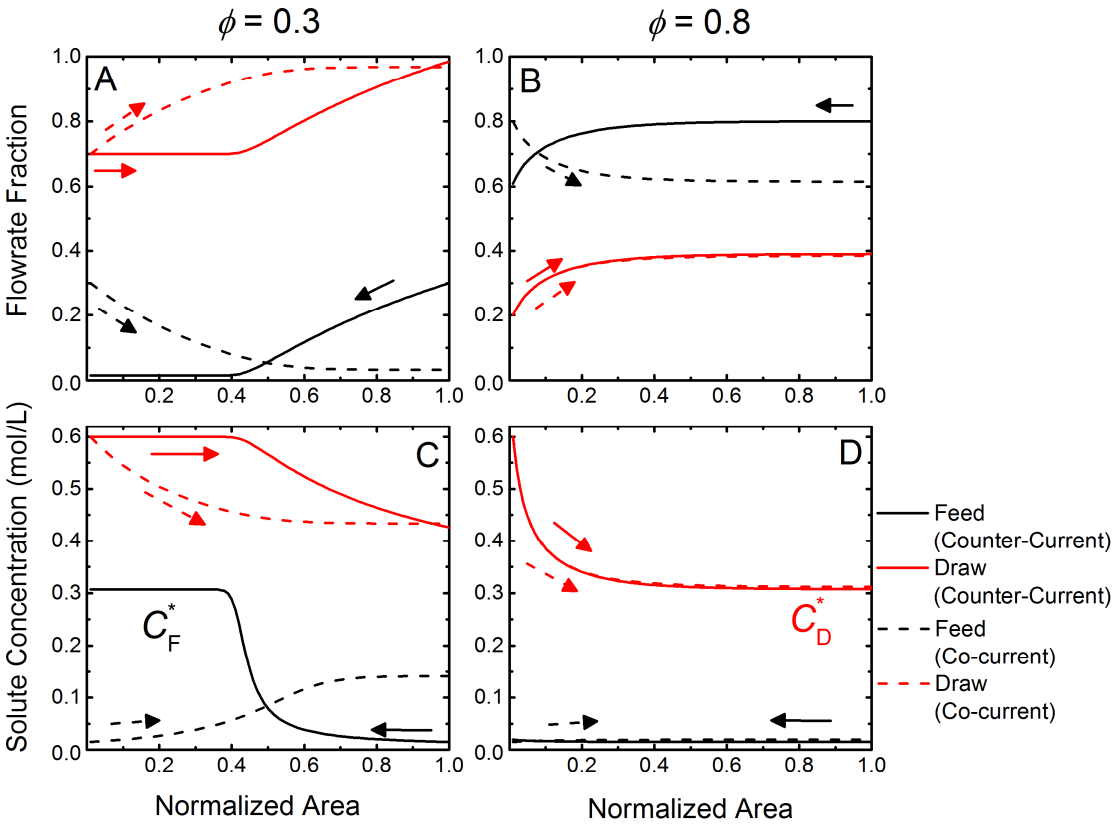

Figure 2

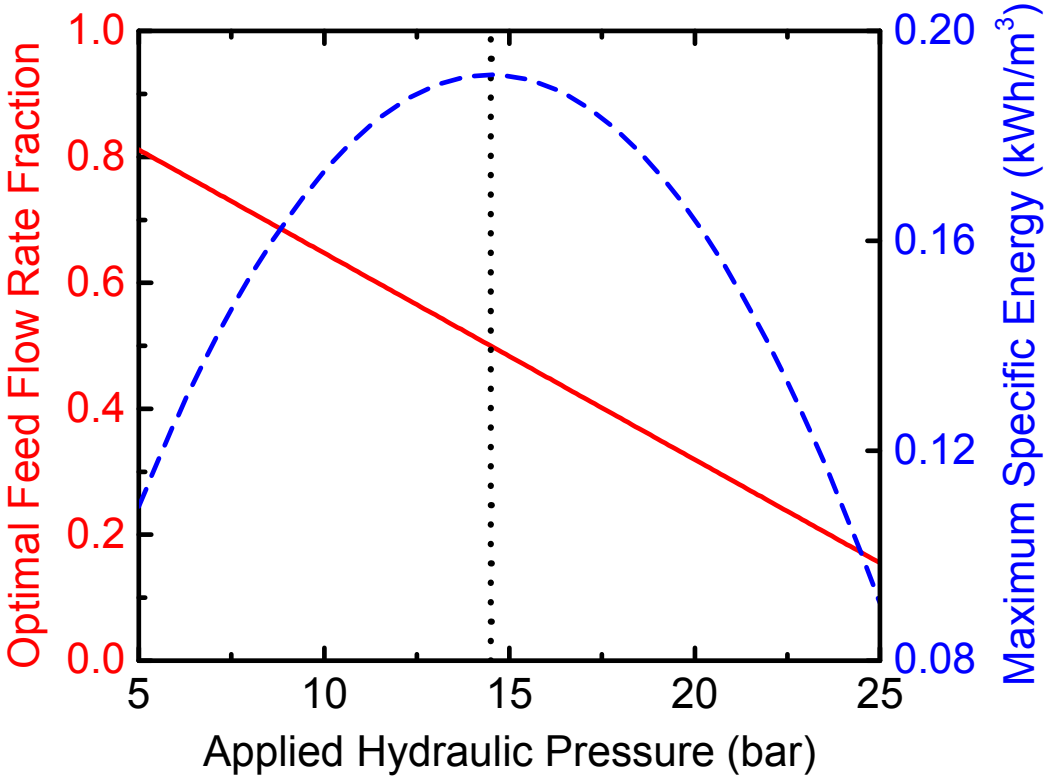

Figure 3

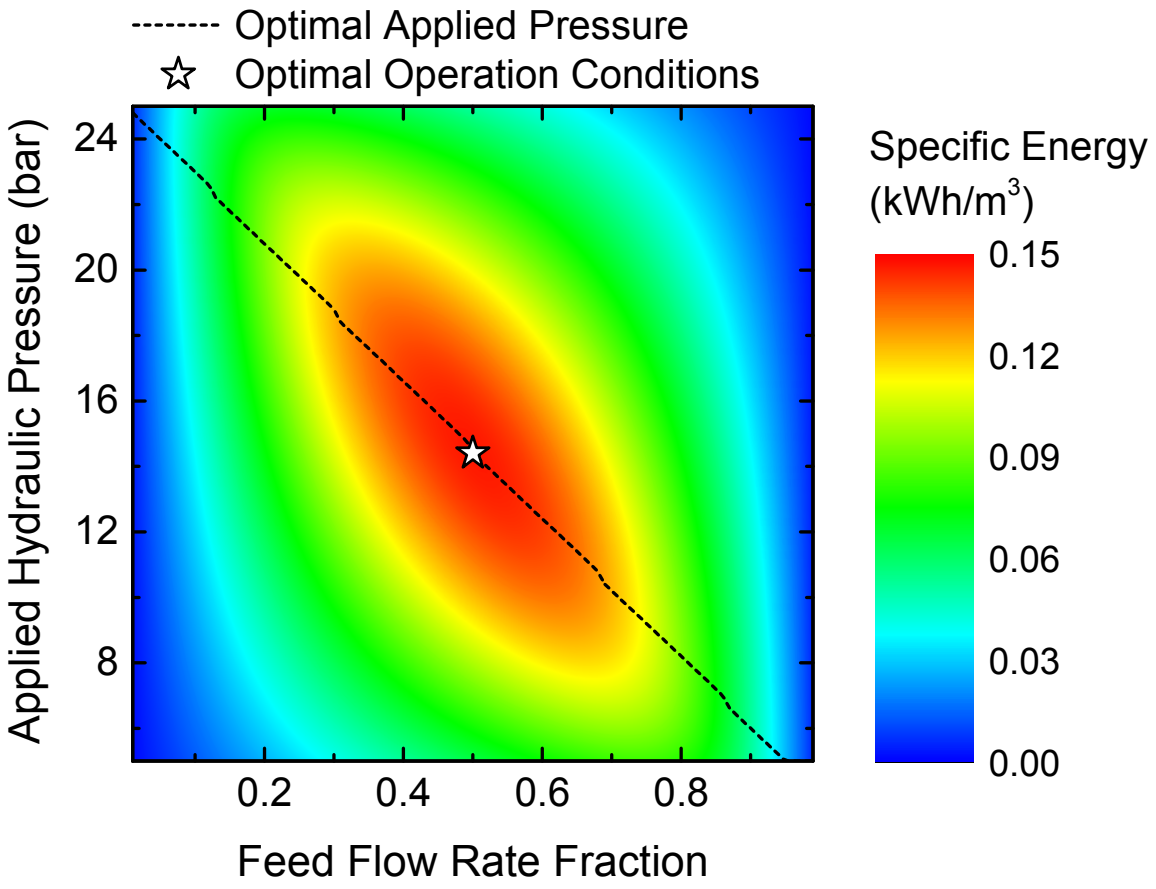

Figure 4

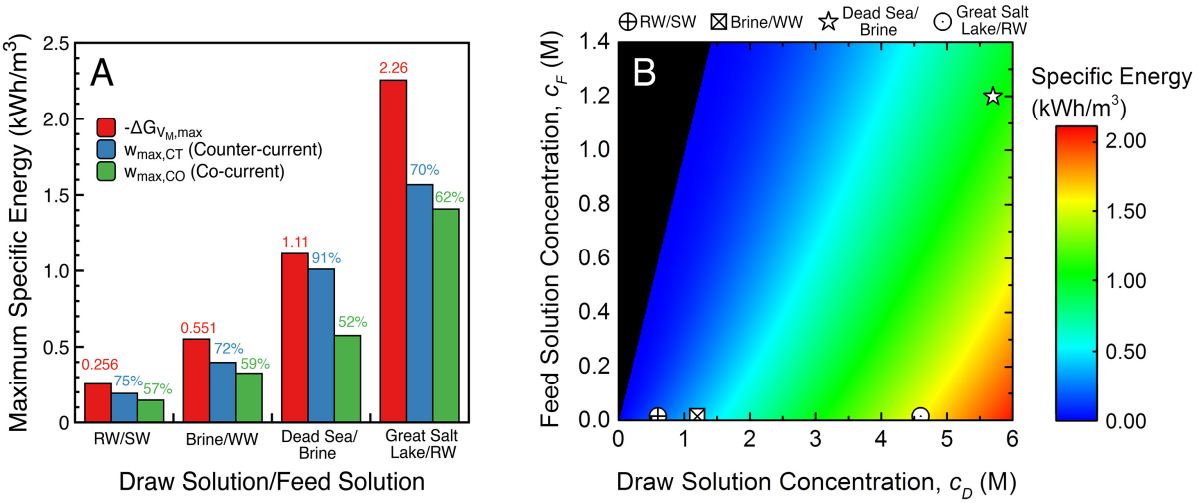

Figure 5